

Facile Synthesis of Ni/Co (Hydr)oxides with Nanosheet Structure for High Performance Supercapacitors

Chengyu Ma¹, Saisai Jian¹, Jinli Qiao^{1,*}, Joey Jung^{2,*}

¹ College of Environmental Science and Engineering, Donghua University, 2999 Ren'min North Road, Shanghai 201620, P. R. China

² Wattech Power Inc, 150-11120 Bridgeport Rd. Richmond BC V6X1T2, Canada

*E-mail: qiaojl@dhu.edu.cn, jjung@wattechpower.ca

Received: 28 August 2016 / Accepted: 2 October 2016 / Published: 10 November 2016

In this article, the novel kind of binary metal oxides, Ni/Co (hydr)oxides, with nanosheet structure have been successfully established via a facile hydrothermal self-assembled process with ammonia solution as the reaction reagent. The as-prepared samples with peculiar morphologies and characteristics are easily realized by just controlling the calcination temperatures. The composition, morphology, and microstructure of the products were characterized by X-ray diffraction (XRD), scanning electron microscopy (SEM), high-resolution transmission electron microscopy (HR-TEM) and X-ray photoelectron spectroscopy (XPS). The thermogravimetric analysis (TGA) revealed the decomposition details of the precursor. Electrochemical measurements show that the sample calcined at 250°C has the optimized capacitive performance, demonstrated by cyclic voltammetry and galvanostatic charge-discharge cycling techniques. The Ni/Co hydroxide nanosheets as electrode materials for supercapacitor exhibit high specific capacitance of 1427 F g⁻¹ at 1 A g⁻¹, and 1270 F g⁻¹ at 10 A g⁻¹, indicating an excellent rate capability. Also, the superior cyclic stability with the capacitance retention of 92.3% is achieved even over 3000 cycles at a high current density of 10 A g⁻¹. The improved capacity and cycling stability makes it promising electrode material for offering an effective way to achieve high supercapacitor performance.

Keywords: Ni/Co (hydr)oxide; Morphology-control; Calcination temperature; Supercapacitor; Cyclic stability

1. INTRODUCTION

In the most recent years, electrochemical capacitors (ECs), also called supercapacitors, have been evoked a great research & development interest in energy/power demanding areas due to their special charge storage mechanisms, and based on which the ECs can be divided into electrical double-layer capacitors (EDLCs) and faradaic capacitors (FCs). Compared to batteries, ECs possess superior

performances such as higher power density, faster charge/discharge rate, longer cycle-life process, better safety assurance and more environmental-friendly[1, 2], which have led ECs to become one of the most promising candidates for next generation energy devices, such as hybrid electric vehicles, power back-up, portable electronic devices or any other devices that require a large amount of power delivered in a very short time[3-5]. However, lower energy densities of ECs than those of batteries and fuel cells still significantly limited their many developments and applications where high energy storage capacities are necessarily required. To overcome this challenge and satisfy the necessary of high energy densities while retaining their intrinsic high power densities and other superior advantages, many efforts have been done especially in the aspect of searching new electrode materials [6-9].

As identified, besides the type of electrolyte solution, electrode material is the key factor affecting the performance especially the energy density of a supercapacitor. As a typical electrode material, RuO₂ has been proved to possess excellent supercapacitive properties. However, its high cost and toxic feature have hindered its widely commercial usage[10, 11]. To further explore more cost-effective, naturally abundant and high performance electrode materials, carbon materials, metal oxides/hydroxides, conducting polymers and hybrid composites have been widely explored as electrode materials for ECs. It is expected that these metal oxides/hydroxides can possess multiple oxidation states which could serve as the active charge storage sites for increasing the capacitance of electrode materials.

Among various electrode materials explored for ECs, Ni and Co oxides/hydroxides and their composites such as NiO[12, 13], Ni(OH)₂ [14, 15], Co₃O₄ [16, 17], Co(OH)₂ [18] and NiCo₂O₄ [19] have drawn increasing attention due to their high capacitance, simple synthesis process and abundance. On the other hand, there is report that the elements of Co and Ni possess the similar structure characteristics, which makes it possible to form hybrid materials to possess better supercapacitive performance in comparison with single metal oxides/hydroxides due to the synergistic effects. This also provided an effective approach to achieve novel electrode materials with excellent electrochemical performances [20-24].

In the synthesis of Ni/Co hydroxides, various approaches, such as sonochemical method [25], microwave-assisted route [26], co-precipitation method[27] and hydrothermal method have been carried out. Among these approaches, the hydrothermal one is considered to be a fast, simple and effective method for synthesizing transition metal hydroxides due to its clean, low-cost and high efficient features. For instance, Hu and his co-workers synthesized the chain-like NiCo₂O₄ with specific capacitance of 1284 F g⁻¹ at the current density of 2 A g⁻¹ by adopting hydrothermal method. Pu et al reported the nickel-cobalt layered double hydroxides nanosheets that were prepared by hydrothermal method to obtain the supercapacitive performance of specific capacitance of 1734 F g⁻¹ at 6 A g⁻¹.

In this paper, we described a facile and reliable method consisted of two steps (hydrothermal reaction followed by a thermal decomposition process (or calcination)) for the production of high-quality Ni/Co (hydr)oxide nanosheets. Unlike previous synthetic methods of nickel hydroxide and cobalt hydroxide[28], in this work, it needs neither any adsorptive surfactant for controlling the morphology structure nor oxidants for producing trivalent cations. Therefore, the large-scale

production of such electrode material can be easily realized. The effect of calcination temperatures on the electrochemical capacitance of the materials is tested to obtain the optimized material composition. A high specific capacitance of 1427 Fg^{-1} at 1.0 Ag^{-1} , a good rate capability (still maintaining 88.99% capacitance in the current density from 1 to 10 A g^{-1}) and excellent cycling stability (only 7.7% loss after 3000 cycles) are achieved when the calcination temperature is around 250°C . The unitary nickel hydroxide and cobalt hydroxide were also synthesized to be compared with the Ni/Co hydroxide nanosheets thoroughly. All the results demonstrate that the Ni/Co hydroxide nanosheets synthesized in this work should be a promising electrode material for supercapacitors.

2. EXPERIMENTAL

2.1 Synthesis of Ni/Co hydroxide nanosheets

All of the chemicals were of analytical grade and used without further purification. Ni/Co hydroxide nanosheets were synthesized by a facile hydrothermal method. In a typical synthesis process, 1.124g $\text{CoSO}_4 \cdot 7\text{H}_2\text{O}$ and 0.525g $\text{NiSO}_4 \cdot 6\text{H}_2\text{O}$ (the molar ratio of Co^{2+} and Ni^{2+} was 2:1) were dissolved in 40 mL deionized water with vigorously stirring to form a pink transparent solution, and then, 10 mL ammonia solution (2.5~2.8 wt.%) was dropwise added into above solution with continuous stirring at room temperature. Then the mixture was transferred into a 100 mL Teflon-lined stainless steel autoclave and maintained at 160°C for 6 hours. After cooling down to room temperature, the precipitate was separated by centrifugation and washed with deionized water and ethanol for several times, afterward dried in vacuum oven at 80°C overnight. The obtained product was then divided into four equal portions and separately annealed at 150, 250, 350 and 450°C for 3 hours in the muffle furnace to further obtain the final products. For a good comparison, the single nickel hydroxide and the cobalt hydroxide were also prepared in which $\text{NiSO}_4 \cdot 6\text{H}_2\text{O}$ or $\text{CoSO}_4 \cdot 7\text{H}_2\text{O}$ was used as the precursor instead of both to prepare the unitary counterpart.

2.2 Characterization

The structure of the Ni/Co hydroxide nanosheets was examined with the help of X-ray diffraction (D/Max-2400) with Cu K α radiation ($\lambda=1.54056\text{\AA}$) operating at 40 kV and 200 mA. TGA of the samples was performed using EXSTAR6200 TGA from SII Nanotechnology Japan at a heating rate of $20^\circ\text{C min}^{-1}$ from 30°C to 600°C . The morphologies of the samples were characterized using the SEM (SEM, HITACHI/S-4800). HR-TEM and selected area electron diffraction (SAED) analyses were performed with a high-resolution Hitachi JEM-2100F operating at 200 kV to obtain the information of the average particle size and the crystal properties of catalysts. XPS were recorded on an ESCA Lab MKII X-ray photoelectron spectrometer with nonmonochromatized Mg K α X-ray as the excitation source. The binding energies in XPS analysis were corrected by referencing C 1s to 285.60 eV.

2.3 Electrode preparation and electrochemical characterization

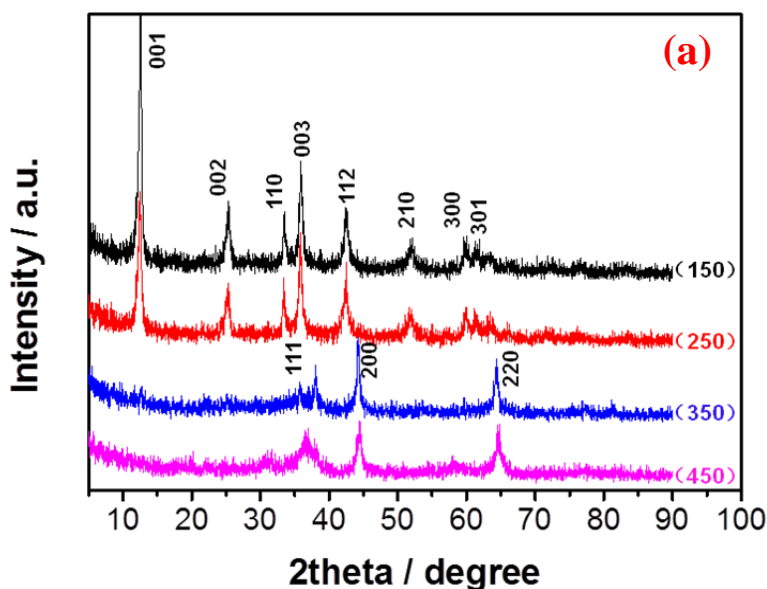
The electrochemical properties of the products were analyzed using a three-electrode electrochemical cell containing N₂-saturated 1 M KOH aqueous solution with a CHI760D electrochemical workstation, (Chenhua Shanghai). The working electrode was prepared by coating an ink layer of Ni/Co (hydr)oxide onto the glassy carbon disk electrode surface. The ink was prepared by mixing Ni/Co (hydr)oxide, acetylene black (AB) and Nafion[®] (Dupont, 0.5 wt.%) with a weight ratio of 8:1:1 in 2mL ethanol. The glassy carbon disk electrode with a geometric area of 0.283 cm² (6 mm diameter) served as the working electrode. The overall loading of Ni/Co (hydr)oxide on the working electrode was 0.5 mgcm⁻². A platinum wire and the saturated calomel electrode (SCE) were used as the counter electrode and reference electrode, respectively.

The cyclic voltammograms were recorded in potential range of -0.15-0.5 V with different scan rates ranging from 10 to 50 mV s⁻¹. Galvanostatic charge-discharge testing was performed in the potential range of 0 and 0.37 V at different current densities from 1 to 10 Ag⁻¹. The cycle-life measurement was carried out for 3000 cycles at a current density of 10 Ag⁻¹ by galvanostatic charge-discharge technique.

3. RESULTS AND DISCUSSIONS

3.1 Material characterization

To characterize the crystal phase of Ni/Co hydroxide nanosheets, powder XRD measurements were carried out. As shown in the Fig. 1(a), when the calcination temperature is below 250°C, the diffraction peaks are almost the same, and the corresponding peaks indicate that cobalt and nickel hydroxides exist as Co(OH)₂ and 4Ni(OH)₂·3H₂O.



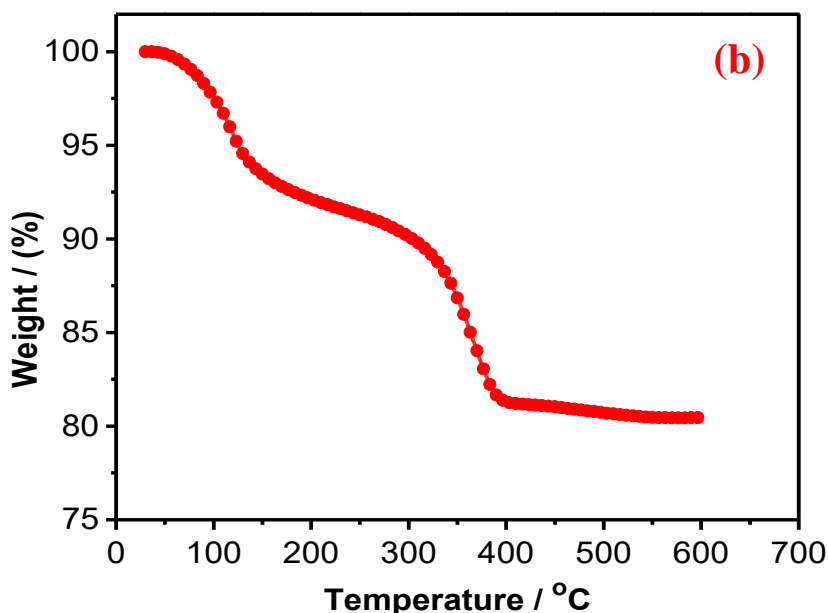


Figure 1. (a) XRD patterns of the as-synthesized nanosheet samples at different reaction temperatures of 150, 250, 350 and 450°C, (b) TGA of uncalcined sample at a heating rate of 20°C min⁻¹ from 30°C to 600°C.

With the similar structure characteristics, the cobalt hydroxide and nickel hydroxide possess the similar diffraction peak positions. Therefore, it is difficult to differentiate between the two phases[29]. When the calcination temperature increases to higher than 350°C, both Ni and Co hydroxides change to Ni oxide and Co oxide due to the loss of the bounded water.

To further illustrate this water loss observed by the XRD study above, TGA test for the samples without annealing was carried out from 30 to 600°C at a heating rate of 20°C min⁻¹. As shown in Fig. 1(b), it can be seen that there exists mainly two-step weight losses. The first sharp weight loss occurs at about 100°C and finished at 150°C, which can be attributed to the loss of absorbed moisture and bound water. The second one appears around 350°C, corresponding to the decomposition of the hydroxides and the complete conversion from Ni/Co hydroxide to Ni/Co oxide. This is also coincident to the XRD analysis.

The morphology of the Ni/Co hydroxide nanosheets are examined by SEM images, where the samples were obtained at 150, 250, 350 and 450°C, respectively. From Fig. 2(a-d), it can be observed that the Ni/Co hydroxide all shows a sheet-like structure. The SEM image of sample obtained at 150°C (Fig. 2(a)) shows almost similar morphology structure to that of 250°C (Fig. 2(b)), and the only difference between them is the sizes and/or thickness of the nanosheets. From Fig. 2(b), one can see that the size of 250°C seems to be much thicker than that of 150°C, which is probably caused by more water loss at 250°C.

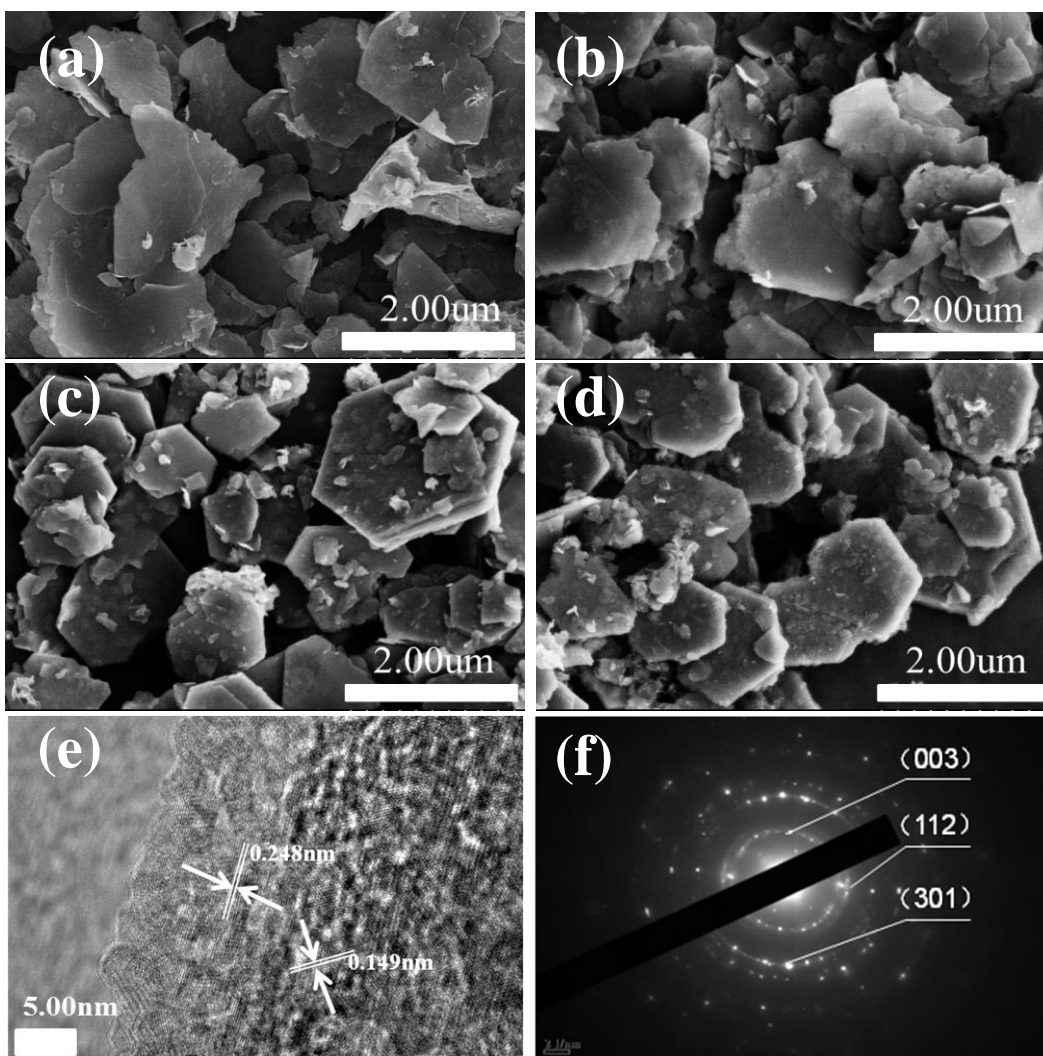
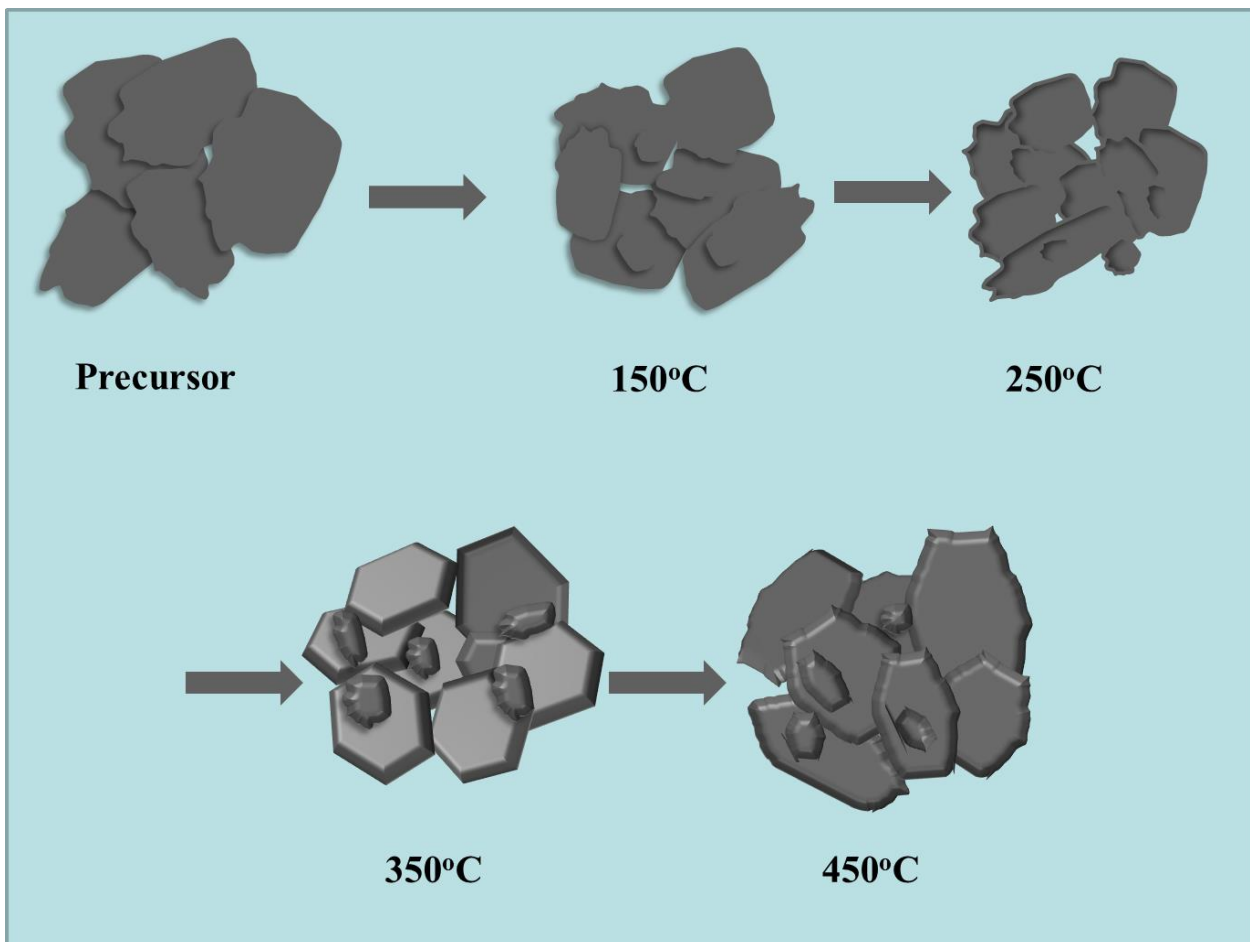


Figure 2. SEM images of the samples collected at different reaction temperatures of (a) 150; (b) 250; (c) 350 and (d) 450°C; (e) HR-TEM image of Ni/Co hydroxide nanosheets annealed at 250°C; (f) selected area electron diffraction (SAED) pattern of Ni/Co hydroxide nanosheets annealed at 250°C.

Combined with the results of the TGA analysis (Fig. 1(b)), it can be concluded that due to water loss at high temperature, the surface of nanosheet could shrink more and even crumpled, thus leading to an increase in its thickness. However, the morphology cannot be changed much when the calcining temperature is below 250°C. Given a careful observation, it is found that the whole morphology seems to be disorderly and irregularly stacked. This may be beneficial to the generation of more sites for the adsorption of ion and efficient pathways for charge transport, which will be discussed further by following electrochemical results. To our interest, when the calcination temperature reaches to 350°C, the nanosheet structure almost disappeared, instead, a novel type of morphology composed of regular hexagon can be clearly observed as shown in Fig. 2(c). At this stage, Ni/Co hydroxide may decompose to form the Ni/Co oxide, which is in a well agreement of the results as indicated by both TGA and the XRD analysis. With further increasing the calcination temperature

high up to 450°C, the regular hexagon begins to collapse again, leading to a disordered and unregulated structure (Fig. 2(d)). Based on the above results, we have made an attempt to further interpret the formation process of the nanosheet like morphology in a pictorial manner. Scheme 1 shows the plausible mechanism for the formation of Ni/Co hydroxide nanosheets.



Scheme 1. Pictorial representation of the mechanism for the formation of Ni/Co hydroxide nanosheets.

In order to further understanding the microcosmic characteristics of as-prepared Ni/Co hydroxide nanosheets, Fig. 2(e) shows the HR-TEM image of Ni/Co hydroxide nanosheets with sample annealed at 250°C as a typical candidate. Fig. 2(e) clearly shows that the lattice phase has random orientation, which demonstrates the polycrystalline nature of Ni/Co hydroxide nanosheets. Lattice fringes can be discerned in the HR-TEM image, and the lattice spacing of 0.248 nm and 0.149 nm are corresponding to the (003) and (301) planes of Ni/Co hydroxide nanosheets, respectively. The SAED pattern (Fig. 2(f)) reveals the defined rings. It is an indication of the polycrystalline nature, which is consistent with the XRD and HR-TEM results. Such polycrystalline nanosheets are expected to possess excellent electrochemical properties.

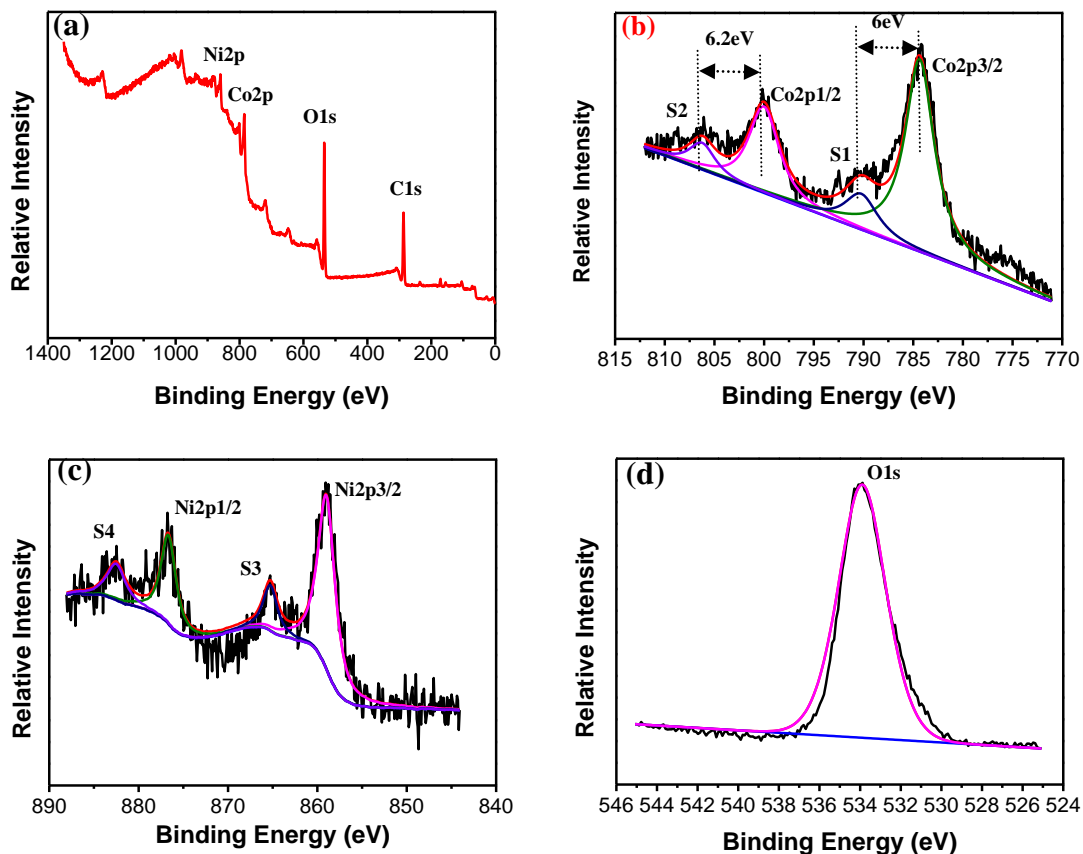


Figure 3. (a) Full XPS spectrum; (b) Co 2p XPS; (c) Ni 2p XPS and (d) O 1s XPS.

The chemical bonding states of each element on the surface of the Ni/Co hydroxide nanosheets were evaluated by XPS technique. A typical survey XPS spectrum of the Ni/Co hydroxide is illustrated in Fig. 3(a), in which Ni, Co, O and C elements are present. The possible variations in oxidation states for Co can be determined from the Co 2p peaks in the XPS spectra. As Fig. 3(b) shows, there are two main spin orbital lines, i.e., 2p_{3/2} and 2p_{1/2} at 784 and 800 eV, respectively in the Co 2p spectrum. Also, two satellite peaks are detected with binding energy about 6 eV (S1) above the 2p_{3/2} main peak and 6.2 eV (S2) above the 2p_{1/2} main peak. Generally, the energy gap between the main peak and the satellite peak is highly related to the oxidation states. It's reported that when the energy gap is about 6.0 eV, the spectrum is associated with Co cations having a valence of 2+[30-32]. Therefore, there is only Co²⁺ cations exist in the Ni/Co hydroxide nanosheets. The Ni 2p line shows four peaks. As can be observed from Fig. 3(c), two associated to the 2p_{3/2} and 2p_{1/2} final states and two correspond to their shake-up satellites. The peaks at 853.8 and 871.3 eV could be assigned to Ni2p_{3/2} and Ni 2p_{1/2}, respectively, and it could be seen clearly that two satellite peaks(S3 and S4) at the high binding energy side of the Ni 2p_{3/2} and 2p_{1/2} edge, which are consistent with literature data for Ni(OH)₂ [33-35]. While in Fig. 3(d) for O 1s spectrum of Ni/Co hydroxide nanosheets, a sharp peak at 533.7 eV can be observed, which is in good agreement with the oxygen in hydroxyl.

3.2 Electrochemical characterization

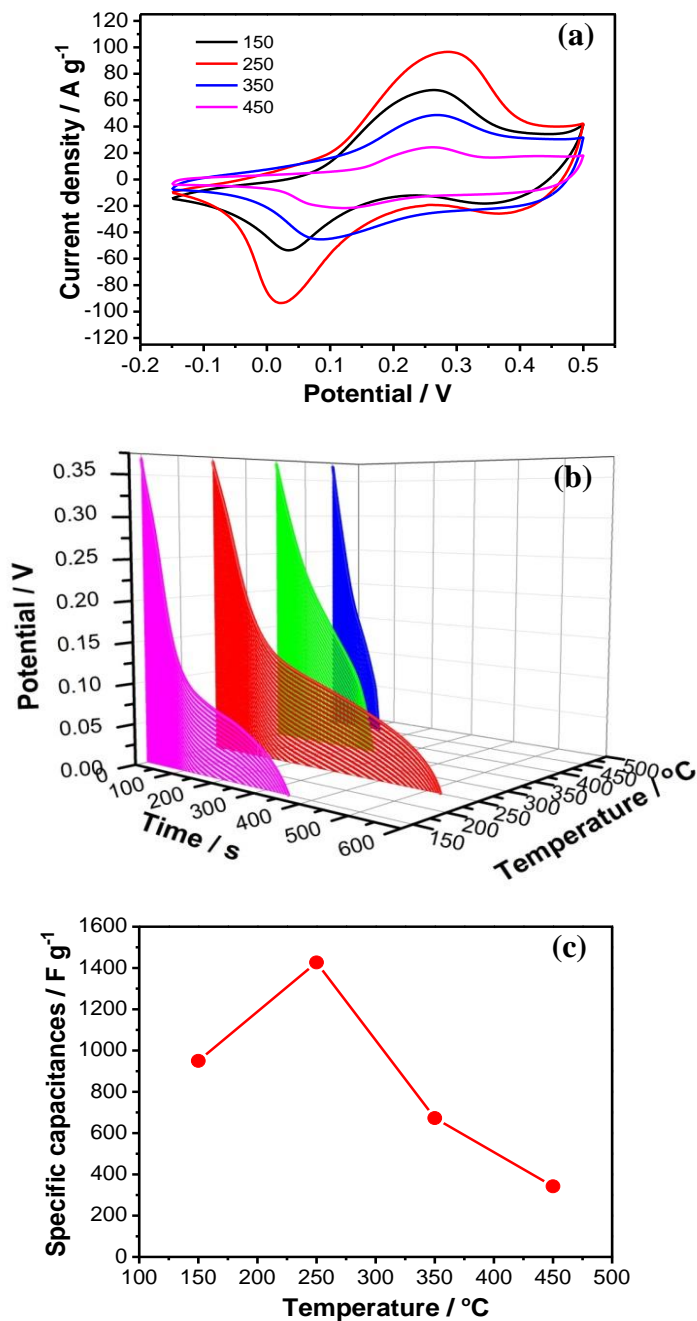


Figure 4. (a) the CV curves of the Ni/Co hydroxide nanosheets in 1 M KOH at a scanning rate of 50 mVs⁻¹; (b) galvanostatic discharge curves for the samples measured between 0 and 0.37 V at current density of 1Ag⁻¹; (c) the specific capacitance of the samples.

To evaluate the electrochemical properties, the sample of Ni/Co hydroxide nanosheets was used to coat the work electrode for the measurements. Fig. 4(a) shows the cyclic voltammograms (CVs) of the Ni-Co hydroxide nanosheets in N₂-saturated 1 M KOH at a scanning rate of 50 mV s⁻¹ in the potential range from -0.15 to 0.5 V. The shape of the CVs indicates that there is an electrochemical

reaction occurs, which can be assigned to a 2-electron transfer process, as reported in literature[1]. This semi-reversible electrochemical reaction can give a high pseudo capacitance of the Ni/Co hydroxide electrode. The electrochemical process can be partially contributed by two reactions ($\text{Co(OH)}_2 + \text{OH}^- \leftrightarrow \text{CoOOH} + \text{H}_2\text{O} + \text{e}^-$, and $\text{Ni(OH)}_2 + \text{OH}^- \leftrightarrow \text{NiOOH} + \text{H}_2\text{O} + \text{e}^-$)[36]. The specific capacitance of the sample can be calculated by using the area under the CV and the specific capacitance of the samples is directly proportional to the area of the CV curves at the same scan rate[37]. From Fig. 4(a), it can be seen that the sample of 250°C possesses the largest area at the same scan rate among all samples. When the calcination temperature goes over 250°C, further increasing temperature makes the CV are a smaller gradually. In other words, the specific capacitance of the samples is reduced with increasing the calcination temperature. Galvanostatic charge-discharge testing is also carried out to further evaluate the capacitive performance. Fig. 4(b) shows the galvanostatic discharge curves for all samples, measured between 0 and 0.37 V at a current density of 1 Ag^{-1} . It can be observed that the sample of 250°C possesses the longest discharge time at the same current density. Based on the galvanostatic charge-discharge testing, the specific capacitance (C) can be calculated according to the equation of $C = \frac{I\Delta t}{m\Delta E}$ (equ 1), where C is the specific capacitance (Fg^{-1}), I the discharge current (A), and m , ΔE and Δt are the mass of active material loading(g), potential range (V), and total discharge time(s), respectively. The obtained specific capacitances for several samples of 150, 250, 350 and 450°C are 950, 1427, 673 and 342 F g^{-1} , respectively. Another specific capacitance calculation method is based on the equation of $C = \frac{2I \int_{E_1}^{E_2} E(t) dt}{m\Delta E^2}$ (equ2)[38, 39], the obtained specific capacitances for several samples of 150, 250, 350 and 450°C are 797, 1044, 657 and 321 Fg^{-1} , respectively. Obviously the results based on equ2 were relatively lower than those based on equ1. And this can be ascribed to the different calculated methods. From Fig. 4(c), it can be seen that in the temperature range from 150 to 250°C, the specific capacitance presented the ascending tendency with increasing the calcination temperature. This increase can probably be attributed to the removal of bound water, which may broaden the pore structure of nanosheet for an easy access of OH^- to the active sites, leading to a fast ion diffusion rate within the redox reaction[40]. However, when the temperature is further increased, the capacitance is gradually decreased with the calcination temperature exceeds 250°C. This may indicate that the initial structure of the sample is gradually changed toward an adverse structure for ion/electron transport. Obviously, when the calcination temperature is at 250°C, the sample can give the best electrochemical performance.

Fig. 5 shows the electrochemical performances comparison of the nickel hydroxide, cobalt hydroxide and the Ni/Co hydroxide nanosheets. The comparison of CV curve average areas further indicates that the as-obtained hybrid nanosheets possess a significantly higher specific capacitance than unitary nickel hydroxide or cobalt hydroxide electrode, as it is generally accepted that the specific capacitance of the samples is directly proportional to the area of the CV curves at the same scan rate.

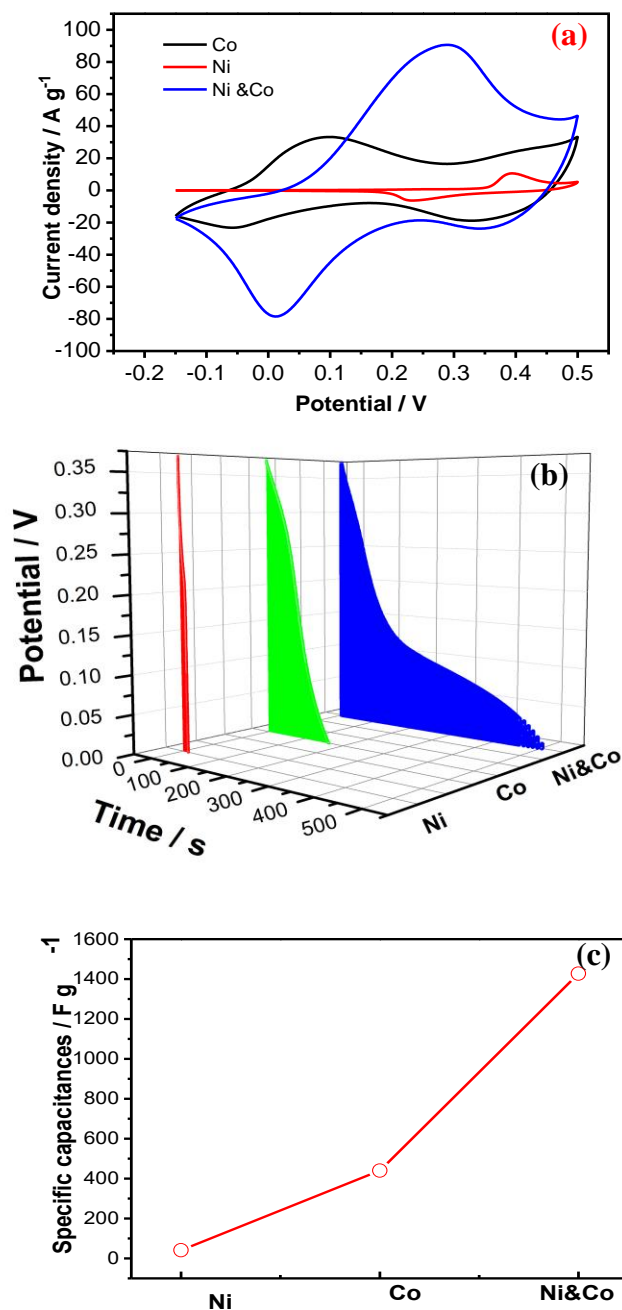


Figure 5. (a) CV curves of thenickel hydroxide, cobalt hydroxide and the Ni/Co hydroxide nanosheets at the scanning rate of 50mV s⁻¹; (b) galvanostatic discharge curves of the samples at the current density of 1Ag⁻¹; (c) the specific capacitances of the samples at a the current density of 1 Ag⁻¹.

As Fig. 5(a) shows, it is obvious that the Ni/Co hydroxide nanosheets possess the largest area in the same scanning rate compared to the single ones. Fig. 5(b) shows the galvanostatic discharge curves for the three samples, measured between 0 and 0.37 V at a current density of 1Ag⁻¹. It is obvious that the Ni/Co hydroxide nanosheets presented the longest discharge time, which is consistent with the results of the CV curves. Based on the equation of $C = \frac{I\Delta t}{m\Delta E}$, the specific capacitances of the

three samples can be calculated and the results are illustrated in Fig.5(c). One can see that the Ni/Co hydroxide nanosheets possesses the largest specific capacitance in exceeding 1400 F g^{-1} , compared to 400 F g^{-1} for single cobalt hydroxide and only 40 F g^{-1} for single nickel hydroxide, respectively. This may be due to the fact that the combination of cobalt and nickel tremendously enlarges the active sites and, the synergies of cobalt and nickel greatly contributed to the super-capacitive properties.

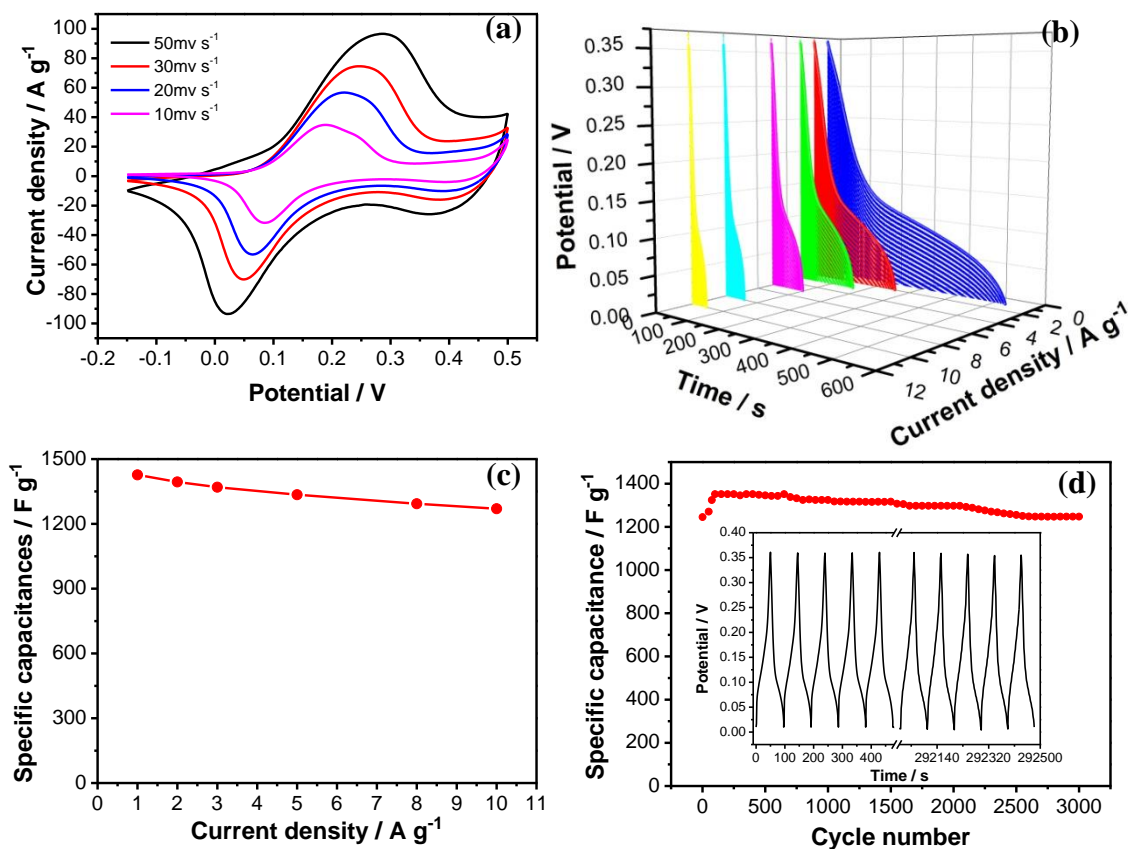


Figure 6. (a) CV curves of the sample synthesized 250°C at a variety of scanning rates ranging from 10 to 50 mV s^{-1} ; (b) galvanostatic discharge curves of the sample synthesized 250°C at different current densities from 1 to 10 A g^{-1} ; (c) the specific capacitances at a variety of current density ranging from 1 to 10 A g^{-1} ; (d) the 3000 cycle life test at a galvanostatic charge-discharge current density of 10 A g^{-1}

To further explore the electrochemical rate performance of the sample Ni/Co hydroxide nanosheets prepared at the calcination temperature of 250°C , the measurements were also carried out at several different potential scan rates from 10 to 50 mV s^{-1} , as seen in Fig. 6(a). It can be seen that the typical pairs of redox peaks possess a good symmetry, indicating that the sample of 250°C has an admirable electrochemical reversibility, which is beneficial to the fast rate performance of the supercapacitor. Furthermore, there is no obvious change of the shape of the CV curves by increasing

the scan rate, and the peak current rises with the scanning rate increasing, indicating that the structure of the sample 250°C is beneficial to fast redox reactions.

Fig. 6(b) displays the galvanostatic discharge curves of the sample of 250°C at different current densities from 1 to 10 Ag^{-1} in the potential range between 0 and 0.37 V. From a further data analysis of Fig. 6(b), the specific capacitances can be obtained as 1427, 1394, 1370, 1335, 1293 and 1270 F g^{-1} at the current densities of 1, 2, 3, 5, 8 and 10 Ag^{-1} , respectively. Based on the equation, the results of the specific capacitances are 1044, 1005, 986, 966, 942 and 926 F g^{-1} , respectively. Although the results are some different based on different calculated methods, the presented trends are accordance with each other. It can be seen that the specific capacitance of the sample of 250°C decreases with increasing the current density. This may be caused by the insufficient diffusion rate of OH^{-} group in the electrode layer. When OH^{-} transfer is slow, more time is needed for transport of the solution into the electrode material surface to access the active sites during charging and discharging process. When the current density is high, such as 10 Ag^{-1} , the OH^{-} does not have enough time to transfer, leading to less charge storage than that at a low current density, thus resulting in a lower specific capacitance. Even though, around 89% of the initial specific capacitance can still be remained at such a high current density of 10 Ag^{-1} , indicating that the sample of 250°C has an excellent rate performance. It should be mentioned that NiCo_2O_4 deposited on functionalized multiwall carbon nanotubes (MWCNTs) has been reported to show a high specific capacitance of 2032 F g^{-1} [41]. Also, the flower-like nickel–cobalt oxide/MWCNTs composites synthesized from hydrothermal method gave a specific capacitance of 1703 F g^{-1} at 1 A g^{-1} , both of which are higher than the as-prepared Ni/Co (hydr)oxides nanosheets in this work. As yet, the addition of the CNTs makes the synthesis approach more complex and cost higher. On the contrary, the facile and low cost synthetic method developed in our work occupies more advantages and competitiveness, which has enabled us to produce batches of electrode materials on gram scales. Therefore, our study may provide a feasible way to produce highly efficient Ni/Co (hydr)oxides nanosheets and can guide future electrode material development.

To evaluate the stability of Ni/Co (hydr)oxides nanosheets, sample of 250°C was tested in further for 3000 cycles of charge/discharge at a galvanostatic current density of 10 Ag^{-1} within the potential window of 0–0.37 V. The results are presented in Fig. 6(d). It can be seen that almost no obvious decreasing in capacitance was observed. Even after 3000 cycles, a high capacitance retention of 92.3% was still achieved, indicating that the Ni/Co (hydr)oxides nanosheets of as-prepared at 250°C possesses an outstanding cycle-life.

4. CONCLUSIONS

In summary, a facile and reliable method containing two steps (a hydrothermal reaction step followed by a calcination step) to synthesize the high-quality Ni/Co hydroxide nanosheets is demonstrated in this work. By changing the calcination temperature, the nanosheets with different morphologies and electrochemical performance are obtained, indicating that the calcination temperature plays an important role in the synthesis of Ni/Co (hydr)oxide nanosheets. The optimum calcination temperature is found to be 250°C, at which the sample can give a substantially improved

electrochemical performance and exhibited the maximum specific capacitance of 1427 F g^{-1} at 1 A g^{-1} . Furthermore, this sample can also give a remarkable capacitance of 1270 F g^{-1} even at the charge/discharge rates of 10 A g^{-1} , indicating that it possesses an excellent rate performance. In addition, the amount of degradation of such as sample is only 7.7% after a cycle-life test for 3000 charge/discharge cycles, demonstrating a good stability of the sample. Due to the low-cost and facile process of the synthesis method, the electrode materials prepared in this work, which have both high capacitance and stability, would be promising for supercapacitor applications.

ACKNOWLEDGEMENTS

This work was financially supported by the National Natural Science Foundation of China (U1510120); the International Academic Cooperation and Exchange Program of Shanghai Science and Technology Committee (14520721900) and the College of Environmental Science and Engineering, State Environmental Protection Engineering Center for Pollution Treatment and Control in Textile Industry, Donghua University.

References

1. G. Wang, L. Zhang, J. Kim, J. Zhang, *J. Power Sources*, 217 (2012) 554.
2. C. Zhong, Y. Deng, W. Hu, J. Qiao, L. Zhang, J. Zhang, *Chem. Soc. Rev.*, 44 (2015) 7484.
3. X. Liu, S. Shi, Q. Xiong, L. Li, Y. Zhang, H. Tang, C. Gu, X. Wang, J. Tu, *ACS Appl. Mater. Interfaces.*, 5 (2013) 8790.
4. M. S. Wu, Z. B. Zheng, Y. S. Lai, J. J. Jow, *Electrochim. Acta.*, 182 (2015) 31.
5. R. Zou, K. Xu, T. Wang, G. He, Q. Liu, X. Liu, Z. Zhang, J. Hu, *J. Mater. Chem. A.*, 1 (2013) 8560.
6. W. Chen, J. Shi, T. Zhu, Q. Wang, J. Qiao, J. Zhang, *Electrochim. Acta.*, 177 (2015) 327.
7. F. Wang, S. Xiao, Y. Hou, C. Hu, L. Liu, Y. Wu, *RSC Adv.*, 3 (2013) 13059.
8. J. Liu, X. Du, Y. Yang, Y. Deng, W. Hu, C. Zhong, *Electrochem. Commun.*, 58 (2015) 6.
9. H. Li, X. Yang, X. Wang, M. Liu, F. Ye, J. Wang, Y. Qiu, W. Li, Y. Zhang, *Nano Energy.*, 12 (2015) 468.
10. K.K. Lee, W.S. Chin, C.H. Sow, *J. Mater. Chem. A.*, 2 (2014) 17212.
11. Z. Wang, Q. Sha, F. Zhang, J. Pu, W. Zhang, *CrystEngComm.*, 15 (2013) 5928.
12. K. K. Purushothaman, I. M. Babu, B. Sethuraman, G. Muralidharan, *ACS Appl. Mater. Interfaces.*, 5 (2013) 10767.
13. G. Anandha Babu, G. Ravi, M. Navaneethan, M. Arivanandhan, Y. Hayakawa, *J Mater Sci: Mater Electron.*, 25 (2014) 5231.
14. J. W. Lang, L. B. Kong, W. J. Wu, M. Liu, Y. C. Luo, L. Kang, *J. Solid State Electrochem.*, 13 (2008) 333.
15. D. P. Dubal, V. J. Fulari, C. D. Lokhande, *Microporous Mesoporous Mater.*, 151 (2012) 511.
16. Y. Song, X. Cai, X. Xu, X. X. Liu, *J. Mater. Chem. A.*, 3 (2015) 14712.
17. X. Gong, J.P. Cheng, F. Liu, L. Zhang, X. Zhang, *J. Power Sources.*, 267 (2014) 610.
18. C. Yuan, L. Hou, L. Shen, D. Li, F. Zhang, C. Fan, J. Li, X. Zhang, *Electrochim. Acta.*, 56 (2010) 115.
19. S. Xu, D. Yang, F. Zhang, J. Liu, A. Guo, F. Hou, *RSC Adv.*, 5 (2015) 74032.
20. G. Chen, S.S. Liaw, B. Li, Y. Xu, M. Dunwell, S. Deng, H. Fan, H. Luo, *J. Power Sources.*, 251 (2014) 338.
21. K. J. Rahul, R. Salunkhe, Sung-won Lee and H. Ahn, *RSC. Adv.*, 2 (2012) 3190.
22. T. Y. Wei, C. H. Chen, H. C. Chien, S. Y. Lu, C. C. Hu, *Adv. mater.*, 22 (2010) 347.
23. J. Liu, W. Hu, C. Zhong, Y. F. Cheng, *J. Power Sources.*, 223 (2013) 165.

24. C. Zhong, W. B. Hu, Y. F. Cheng, *J. Power Sources.*, 196 (2011) 8064.
25. M. Vidotti, R. P. Salvador, E.A. Ponzio, S. I. Córdoba de Torresi, *J.Nanosci. Nanotechnol.*, 7 (2007) 3221.
26. H. Y. Hsu, K. H. Chang, R.R. Salunkhe, C. T. Hsu, C. C. Hu, *Electrochim. Acta.*, 94 (2013) 104.
27. L. Kong, L. Deng, J. Lang, X. Ji, Y. Luo, L. Kang, *Chinese J. Chem.*, 30 (2012) 570.
28. H. Chen, L. Hu, M. Chen, Y. Yan, L. Wu, *Adv. Fun. Mater.*, 24 (2014) 934.
29. X. Zheng, Z. Gu, Q. Hu, B. Geng, X. Zhang, *RSC. Adv.*, 5 (2015) 17007.
30. D. Barreca, C. Massignan, *Chem. Mater.*, 13(2001) 588.
31. B. Babakhani, D. G. Ivey, *Electrochim. Acta.*, 56 (2011) 4753.
32. F. Yang, J. Yao, F. Liu, H. He, M. Zhou, P. Xiao, Y. Zhang, *J. Mater. Chem. A.*, 1 (2013) 594.
33. P. Liu, Z. Hu, Y. Liu, M. Yao, Q. Zhang, *J. Alloys Compd.*, 622 (2015) 805.
34. M. M. Natile. A. Glisenti, *Chem. Mater.*, 2002, 14, 4895.
35. J. H. Zhong, A. L. Wang, G. R. Li, J. W. Wang, Y. N. Ou, Y. X. Tong, *J. Mater. Chem.*, 22 (2012) 5656.
36. S. K. Meher, P. Justin, G. R. Rao, *Nanoscale.*, 3 (2011) 683.
37. M. Li, K.Y. Ma, J.P. Cheng, D. Lv, X.B. Zhang, *J. Power Sources.*, 286 (2015) 438.
38. A. Laheäär, P. Przygocki, Q. Abbas, F. Béguin, *Electrochem. Commun.*, 60 (2015) 21.
39. S. E. Chun, B. Evanko, X. Wang, D. Vonlanthen, X. Ji, G. D. Stucky, S.W. Boettcher, *Nat. Commun.*, 6 (2015) 7818.
40. Y. Y. Liang, S. J. Bao, H. L. Li, *J. Solid Electrochem.*, 11 (2006) 571.
41. I. Shakir, *Electrochim. Acta.*, 132 (2014) 490.

© 2016 The Authors. Published by ESG (www.electrochemsci.org). This article is an open access article distributed under the terms and conditions of the Creative Commons Attribution license (<http://creativecommons.org/licenses/by/4.0/>).